Published in final edited form as:
Osteoarthritis Cartilage. 2014 February ; 22(2): 275–283. doi:10.1016/j.joca.2013.11.013.

Deleterious effects of osteoarthritis on the structure and function of the meniscal enthesis

A.C. Abraham[†], **H.M. Pauly**[‡], and **T.L. Haut Donahue**[†,*]

A.C. Abraham: acabraha@engr.colostate.edu; H.M. Pauly: hmpauly1@gmail.com; T.L. Haut Donahue: tammy.donahue@colostate.edu

[†]Department of Mechanical Engineering, Colorado State University, Fort Collins, CO 80523, USA

[‡]School of Biomedical Engineering, Colorado State University, Fort Collins, CO 80523, USA

SUMMARY

Objective—The ability of menisci to prevent osteoarthritis (OA) is dependent on the integrity of the complex meniscal entheses, the attachments of the menisci to the underlying subchondral bone (SB). The goal of this study was to determine mechanical and structural changes in meniscal entheses after the onset of OA.

Design—Healthy and osteoarthritic meniscal entheses were evaluated for changes in histomorphological characteristics, mineralization, and mechanical properties. Glycosaminoglycans (GAG) and calcium in the insertion were evaluated with histological staining techniques. The extent of calcium deposition was assessed and tidemark (TM) integrity was quantified. Changes in the mineralized zone of the insertion were examined using micro-computed tomography (μCT) to determine bone mineral density, cortical zone thickness, and mineralization gradient. Mechanical properties of the entheses were measured using nano-indentation techniques to obtain material properties based on viscoelastic analysis.

Results—GAG thickness in the calcified fibrocartilage (CFC) zone and calcium content were significantly greater in osteoarthritic anterior meniscal entheses. TM integrity was significantly decreased in OA tissue, particularly in the medial anterior (MA) enthesis. The mineralized zone of osteoarthritic meniscal entheses was significantly thicker than in healthy entheses and showed decreased bone mineral density. Fitting of mineralization data to a sigmoidal Gompertz function revealed a lower rate of increase in mineralization in osteoarthritic tissue. Analysis of viscoelastic mechanical properties revealed increased compliance in osteoarthritic tissue.

Conclusions—These data suggest that significant changes occur at meniscal enthesis sites with the onset of OA. Mechanical and structural changes in meniscal entheses may contribute to meniscal extrusion, which has been shown to increase the progression of OA.

Keywords

Graded tissue interface; Mechanical properties; Histomorphometry; Tidemark; Root Insertions

[*]Address correspondence and reprint requests to: T.L. Haut Donahue, Department of Mechanical Engineering, Colorado State University, Fort Collins, CO 80523, USA.

Author contributions

Adam Abraham and Tammy Haut Donahue were responsible for conception and design of the study. Tammy Haut Donahue supervised the project. Adam Abraham and Hannah Pauly acquired and analyzed all data. Adam Abraham, Hannah Pauly, and Tammy Haut Donahue interpreted results, performed statistical analysis and drafted and edited the manuscript.

Conflict of interest

The authors have no conflict of interest to disclose.

Introduction

The menisci of the knee joint aid in stability, lubrication, and load distribution, and are comprised of inhomogeneous collagen fiber layers[1]. When the knee is loaded the menisci experience high levels of compressive and shear forces at the articularing surface of the joint. The hierarchical morphology of collagen fibers in the meniscus mainbody allows for the transduction of applied compressive and shear forces into tensile hoop forces. Meniscal attachments, or entheses are graded tissue interfaces that anchor the mainbody of the meniscus to the underlying subchondral bone (SB). Each of the four meniscal enthesis in the knee joint function to diffuse tensile loads which are transmitted, *via* collagen fibrils, from the mainbody of the meniscus[1-7]. In order to effectively attenuate joint loads each enthesis must remain firmly rooted to the tibial plateau[8-10]. Identified enthesopathies at other tissue interfaces have revealed a variety of structural degenerations that may jeopardize enthesis functionality[7,11,12]. Clinically, if a meniscal enthesis is torn or avulsed, excessive transverse meniscal extrusion results[9]. Meniscal extrusion has been shown to be a precursor of secondary osteoarthritis (OA)[13,14]. Individuals with primary OA have also presented with meniscal extrusion, indicating a progressive degeneration of the meniscal enthesis[14-16]. To date, there have been no investigations on the integrity of meniscal entheses in the arthritic knee.

Similar to other fibrocartilaginous entheses, the meniscal entheses are compositionally graded to withstand a myriad of interfacial loading mechanisms. Primarily type I collagen fibrils, extending from the mainbody of the meniscus, form a ligamentous (LI) zone which sustains longitudinal tensile forces manifested by compression on the meniscus[5,17]. These fibers then join with type II collagen fibers forming interwoven uncalcified and calcified fibrocartilage zones (UFC and CFC, respectively), separated by a tidemark (TM)[2,6,18]. These proteoglycan rich zones withstand compression and shear generated by dynamic changes in fiber angle and avulsion stress shielding[7]. Lastly, the CFC zone joins the SB at an interdigitated cement line[2,6,18]. These four zones can vary in size at each meniscal enthesis site, presumably structurally adapting to their unique functional environment[2,6,18]. Coupling mechanical and magnetic resonance imaging studies typifies this as the posterior sites, known to translate more during flexion, are significantly more compliant than the anterior sites[19-21].

Examination of joint and enthesis degeneration identifies various stimuli that may influence insertion mechanics. Regulation of inflammatory and anabolic cytokines can have detrimental effects on ECM integrity. In the OA joint increased production of aggrecanase, resulting in proteoglycan cleavage, and matrix metalloproteinase-13, causing irreversible degeneration of type II collagen, erodes the structural and mechanical efficacy of articular cartilage. The osteochondral interface also exhibits demonstrable changes in mineralization state and integrity, dependent upon disease progression[22,23]. Similarly, ligament and tendon pathophysiology at various insertion sites in the body exhibit ECM disruption, TM breakdown, micro-fissures, and osteophyte formation which impact structural organization and functionality[7]. Assimilating these findings gives rise to the supposition that the meniscus-to-bone interface is a potential disease-forming pathway, possibly preceding or catalyzing other harbingers of degradation.

In this study we examined meniscal entheses from normal and osteoarthritic knees for changes in histomorphometry, mineralization, and mechanical properties. Our hypothesis was that osteoarthritic entheses would exhibit deleterious effects similar to those observed at degenerative tissue interfaces in other articulating joints. These pathologies include breakdown of the TM; clefts and micro-fissures; osteophyte formation; calcium deposition

and increased GAG content in the soft-tissue; and changes in mineralization. These changes would then result in degeneration of the viscoelastic properties of the entheses, thereby contributing to meniscal extrusion.

Methods

Sample preparation

Tissue samples were collected over 1 year based on several exclusion criteria. End-stage osteoarthritic tissue was obtained from patients undergoing total knee arthroplasty who signed an institutional review board approved waiver. Samples were included only if all four meniscal entheses could be identified by gross inspection. This resulted in seven total samples ($n = 7$). Healthy tissue was obtained from the Mayo Clinic tissue donor program. Selection was based on fluoroscopic evaluation and visual inspection by an orthopedic surgeon for no apparent signs of degeneration, and a donor age of <65 years. This resulted in eight total samples ($n = 8$, ages 41–61, average: 55). All samples were obtained with institutional review board approval.

All meniscal entheses (medial anterior (MA), lateral anterior (LA), medial posterior (MP), and lateral posterior (LP)) were excised and bisected along the main fiber axis. Adaxial (AD) sections, used for histomorphometry, were fixed in 10% neutral buffered formalin, serial dehydrated in ethanol, defatted in xylene and then embedded in methyl methacrylate (Technovit 9100 New, Heraeus Kulzer GmbH, Wehrheim, Germany). Abaxial (AB) sections, used for micro-computed tomography (μCT) and indentation, were embedded in a high viscosity acrylic resin (ClaroCit, Struers Inc., Cleveland, OH) that did not penetrate the specimen, wrapped in phosphate buffered saline soaked gauze, and stored at −20°C.

Histomorphometry

Histological sections (30 μm thick) were made using standard cutting and grinding techniques. Samples were stained with toluidine blue (TB) to identify GAGs and then counterstained using the Von Kossa (VK) technique for calcium. Changes in GAG presence in the insertion zones were quantified using Bioquant software (Bioquant Osteo 12.5, Bioquant Image Analysis Corporation, Nashville, TN) to identify the thickness of the TB stained and the TB + VK stained regions. Each region was outlined and measurements were performed at 20 μm intervals. TM integrity was assessed quantitatively. First the TM was isolated using image processing software (Image J), upper and lower color thresholds were determined using intensity histograms and visual inspection of a subset of images. Threshold values were then kept fixed and all images were converted to a binary image, and pixel locations were stored. A custom written Matlab script (version 7.14 (R2012a), Natick MA) then determined the variance of the first derivative and the mean amplitude of the peaks/valleys, estimating TM smoothness. Calcium deposition was scored using a modified grading scale as described by Sun *et al*. 2010[24]. Briefly, deposits were scored on a scale of 0–4 with 0 being no calcium and 4 being large deposits within and around the fibrous insertion.

μCT

The bisected insertions were scanned in saline *via* μCT (Scanco μCT 80, Scanco Medical AG, Brüttisellen, Switzerland) using the following parameters: voltage: 55 kVp, current: 114 μA, integration time: 500 ms. A resolution of 18 μm was obtained, yielding approximately 250 axial slices per specimen. The area of insertion was visually determined using the original specimen and multiple scanned views as reference. Tissue mineral density measurements ($mgHA/cm^3$) across the TM were obtained using Image Processing Language (Scanco Medical AG, Brüttisellen, Switzerland). For each specimen density measurements

were taken at the center of the insertion and 54 μm above and below the center line (Fig. 1). Three additional measurements were taken 54 μm deeper into the initial reference plane, analogous to the tissue depth penetrated by the indenter tip (Section 2.4). A custom Matlab script was used to identify the first peak value of density measurements, which was considered to be indicative of mineralization at the TM, and the values across the TM were averaged for each specimen. The thickness of the cortical shell of each insertion was determined by calculating the number of data points over which the initial density peak occurred. Multiple measurements were taken 28 μm apart extending up and down from the center of each insertion to avoid inadvertently taking measurements through only trabecular struts or voids. The number of measurements for each insertion varied from 6 to 18 depending on the size of the insertion. A custom Matlab script was used to average the lengths of the initial peak of density measurements to quantify the cortical thickness of each insertion. Additionally, the rate of increase in mineral density at the soft-tissue to bone interface was examined. For each sample the mineralization measurements from the initial point of mineralization until the peak mineral density were fit to a sigmoidal Gompertz function such that:

$$\text{Mineral Density}\,(x)=Ae^{Be^{Cx}}$$

where *A* is the upper asymptote (peak density), *B* is the shift along the *x*-axis, and *C* is the mineralization gradient. The resulting coefficients were averaged for each insertion site. This specific formulation of the generalized logistic function was selected as there is a sharp increase in mineral content followed by a gradual maturation to peak mineralization.

Indentation

Indentation was accomplished using a commercial nanoindenter (MTS Nanoindenter XP) with a 300 μm spherical ruby tip. Creep testing was performed using a trapezoidal loading profile with a max load of 1-, 5-, or 10-mN depending if the indentation location was in the LI, UFC or CFC, or SB zone, respectively. Each sample had forty-five test locations selected by establishing the TM and creating three columns of fifteen rows. Column spacing was 50 μm and row spacing was 10-, 50, or 100-μm depending on the zone (Fig. 1). Previous testing performed by our laboratory has shown that the entheses exhibit time-dependent material performance[20], therefore material properties were determined based on the viscoelastic analysis of Oyen[25,26]. For the general case of creep displacement, when time *t* is greater than the rise time τ_R, is

$$h\,(t)=\left[\left(\frac{1}{a}\right)\left[C_0\,\dot{P}\tau_R-\sum_{i=1}^{n}\left[C_i\tau_i\dot{P}e^{-t/\tau_i}\left(e^{\tau_R/\tau_i}-1\right)\right]\right]\right]^{\frac{1}{m}},\ \text{for}\ t\geq\tau_R$$

where C_i and τ_i are creep compliance coefficients and time constants, respectively. The variables *a* and *m* pertain to tip geometric factors, for the explicit case of spherical indentation with tip radius *r*, $a = 8r/3$ and $m = 3/2$. Lastly, the term $\dot{P} = P_{\max}/\tau_R$ refers to the rate of loading from the initial ramp phase. For all data $i = 2$ was found to provide a quality fit to displacement-time histories. The creep compliance coefficients were utilized to compute the instantaneous $(G_0=1/(2(C_0-\sum_{i=1}^{n}C_i)))$ and equilibrium ($G_\infty = 1/(2C_0)$) shear moduli. These properties, computed from an assumption of incompressibility were then converted to a shear modulus with a constant and compressible assumption for Poisson's ratio such that $G^{\nu}_{0,\infty}=2G_{0,\infty}\,(1-\nu)$ where $\nu = 0.3$[27-29]. Shear modulus was converted to elastic modulus using $E_{0,\infty}=2G^{\nu}_{0,\infty}\,(1+\nu)$. Lastly, the tip diameter chosen is

larger than specific zones of the attachment sites, however, the probe only penetrates so far as to produce a ~50 μm contact diameter in the most compliant tissues. The very blunt tip profile was selected in order to reduce variability due to surface roughness, a potential problem with the minimally processed surface[30]. This does result in overlap between indentation sites, and potentially material zones. However, this modality was selected in order to probe if the spatially averaged gradient of material properties across the interface was altered due to OA and should be considered solely in that context and not as a definitive material property for each individual constituent.

Statistical analysis

Eight independent patients contributed to the healthy group and seven independent patients contributed to the OA group. For statistical analyses each of the four entheses for each joint examined were considered an independent sample within each group, healthy ($N = 8$ knees) and OA ($N = 7$ knees). This assumption was made as each enthesis is subject to a unique loading environment throughout joint motion[21]. This, presumably, drives their particular mechanical development and may pattern their degeneration[31].

Differences in calcium deposition between groups were evaluated using a Wilcoxon rank sum test (disease state, level of significance $\alpha = 0.05$). Differences in TM integrity (variance of the first derivative and mean peak amplitude) and GAG thickness (UFC and CFC) were each independently evaluated between groups using a two-sample *t*-test with unequal sample sizes ($\alpha = 0.05$). Differences in the μCT derived parameters cortical shell thickness and bone mineral density were independently evaluated between groups using a two-sample *t*-test with unequal sample sizes ($\alpha = 0.05$). Additionally, the differences between individual fitting coefficients of the Gompertz function were evaluated between groups using a two-sample *t*-test with unequal sample sizes ($\alpha = 0.05$). Lastly, differences between the healthy and OA elastic moduli obtained from the indentation experiments were evaluated separately for each enthesis using two-way repeated measures analysis of variance (location, disease state, $\alpha = 0.05$) and Fisher's least significant difference *post hoc* test. All statistical analyses were performed using Minitab statistical software (Minitab 16, Minitab Inc., State College, PA). All data are expressed as means with 95% confidence interval (lower limit, upper limit).

Results

Histomorphometry

GAG thickness in the UFC regions were not significantly different between healthy and OA tissue. However, there was an increase in GAG thickness in the CFC regions. Specifically, there was significantly more thickness in the LA ($P = 0.027$), MA ($P = 0.028$), and MP entheses ($P = 0.002$) (Table I). TM organization was significantly reduced in osteoarthritic tissue, as evident from the appearance of repeated TMs, osteophytes, and micro-fissures [Fig. 2(D), (E) & (F)]. This was most apparent in MA enthesis as indicated by the increase in the variance of the first derivative ($P = 0.028$) and mean peak amplitude ($P = 0.029$) (Table I). Lastly, there was a significant amount of calcium deposition in both the medial ($P = 0.037$) and lateral ($P = 0.002$) anterior entheses (Table I, Fig. 2).

μCT

Meniscal insertions in patients with end-stage OA had significantly thicker zones of mineralization (740.09 μm, 662.28, 817.89) relative to healthy tissue (401.37 μm, 371.11, 431.30) ($P < 0.0001$). Bone mineral density was significantly lower for osteoarthritic samples (936.25 mgHA/cm^3, 897.93, 974.58) compared to healthy (1023.63 mgHA/cm^3, 999.89, 1047.38) ($P = 0.0004$). When comparisons were made between healthy and

osteoarthritic samples at specific entheses several relative differences were found. Thickness of the mineralized zone at all four locations of osteoarthritic insertions was significantly larger relative to respective healthy insertions (LA: $P = 0.0041$, LP: $P = 0.0017$, MA: $P = 0.0047$, MP: $P < 0.0001$) (Table II). Additionally, when compared to healthy samples the bone mineral density of osteoarthritic insertions was significantly lower for LA, ($P = 0.012$), MA ($P = 0.012$), and medial posterior insertions ($P = 0.28$) when compared to the respective healthy samples (Table II). The sigmoidal function used to describe mineral density as a function of position provided a good fit to the data as it failed to reject the null hypothesis that the mean of the standard variance is zero (Fig. 3). Although there were no statistical differences, in general the rate of increase in mineralization was lower for arthritic tissue, as indicated by the C coefficient (Table III). The LA exhibited the greatest discrepancy in mineralization rate between healthy and OA tissue (Table III).

Indentation

Mechanical evaluation of viscoelastic properties of the entheses revealed a significant decrease in instantaneous and equilibrium elastic moduli in osteoarthritic tissue (Figs. 4 and 5). Specifically, the LA ($P = 0.0008$) and MA ($P < 0.0001$) entheses were most affected by OA. Furthermore this degeneration appeared to be primarily localized to the fibrocartilaginous zones (Figs. 4 and 5). In the LA this was solely in the mineralized tissue, wherein the instantaneous and equilibrium elastic modulus were decreased by half. For the MA there was an even greater discrepancy, as the instantaneous elastic moduli was up to three times higher in healthy tissue for both mineralized and unmineralized regions (Fig. 4). For the equilibrium modulus the relative difference between tissues was the same, however it was only for the mineralized tissue (Fig. 5).

Discussion

To our knowledge this is the first study to examine pathophysiology of the meniscal entheses. Qualitatively, the entheses exhibited morphological changes including a breakdown of TM organization, double TM formation, clefts and microcracks/fissures, osteophytes, and calcium deposition within the soft-tissue, all of which disrupt functional homeostasis. Quantitatively, the arthritic tissue was found to have significant increases in GAG thickness in the mineralized fibrocartilage, cortical shell thickness, peak and mineral density and mineralization gradient, and mechanical compliance. As there is limited data specifically on the meniscal entheses these findings must be considered in the context of other enthesopathies.

Histologic examination of patients with patellar tendinosis reveals an accruement of GAGs at the tissue interface[32]. Similarly, internal obturator tendons removed from osteoarthritic hip joints have significantly more GAGs as well as calcium deposits[33]. These findings implicate swelling of the enthesis that may be an adaptation to increased loading, however this would also result in disruption of the fibrous matrix and effective load transmission. Calcium deposition also plays an integral role in OA pathology as mineral aggregation has been shown in the articular cartilage, meniscus, and synovial fluid[24,33,34]. In our study calcium deposits were observed within the LI zone, potentially disrupting fiber organization and undermining mechanical efficacy. The presence of such deposits is also linked with stimulation of inflammatory and catabolic responses in articular cartilage, thereby contributing to intrinsic degradation[34].

TM integrity is also thought to be crucial for maintaining enthesis functionality[35-37]. Previous evaluation of TM integrity has remained strictly qualitative; however, the metrics introduced here facilitated quantitative comparisons between healthy and arthritic tissue at each enthesis. In general, OA entheses exhibited higher variance and mean amplitude,

suggesting a less organized TM. Specifically, the MA had a significantly greater amount of disorganization, potentially leading to detrimental bone formation extending into the soft-tissue including to osteophyte formation[11,12]. These enthesophytes, distinct from the calcium deposits, commonly appear in the Achilles tendon in athletes. However their direct ramifications are unclear as patients can be asymptomatic[7]. In articular cartilage, osteophyte detection is associated with disruption of the adjacent articulating surfaces thereby exacerbating adverse joint mechanics[38].

Changes in the TM and osteophyte detection are frequently indicative of accompanying bone related OA pathogeneses including thickening of the periarticular bone[23]. The μCT analyses performed reveals similar changes in the cortical shell, inclusive of both the CFC and the SB. Osteoarthritic meniscal entheses demonstrated a significant increase in thickness of the cortical shell relative to healthy insertions. This increase in thickness may occur as a result of increased stresses in the region due to load bearing and a decrease in overall bone mass[39]. Changes in cortical thickness have been known to alter cartilage mechanics and cortical shell thickening may similarly result in altered mechanics of the entheses[23]. It is difficult to assess whether or not the progression of OA results in ultimate thickening of the cortical shell because the initiation point of disease in the tested specimens is unknown. It has been suggested that if OA was initiated as a result of trauma the cortical thickening may be a response of the enthesis to meniscal damage[40]. Furthermore, thickening of the cortical shell occurs simultaneously with a decrease in average bone mineral density[41]. Overall bone mineral density has been shown to decrease as the rate of bone remodeling increases leading to incomplete mineralization[38]. Similarly, there was a significant decrease in mineral density in osteoarthritic samples.

The gradation of mineral content when traversing the TM is of particular interest as it has been shown to influence enthesis mechanics[42,43]. Existing literature suggests a linear increase in mineral content; however, this would appear an oversimplification as the mineralization appears nonlinear during its growth and asymptotic at its extremes[43]. We instead chose a sigmoidal function that could account for no mineralization in the soft-tissue and the nonlinear growth and gradual maturation of mineral density once deep enough into the calcified tissue. There are trending differences in fitting coefficients between attachment sites and healthy and OA tissue. The B & C coefficients of the sigmoidal function are indicative of a more gradual start to mineralization and progressive increase in mineral density, respectively. Between healthy attachment sites it is evident that the MA enthesis begins to mineralize sooner however the rate of mineralization is more gradual across the interface. The early initial mineralization of the MA enthesis may be attributable to the thinner cortical zone of the insertion[2,6]. OA appears to slightly decrease the rate of mineralization across the interface, particularly in the LA enthesis. This could have profound effects on stress dissipation across the enthesis as, above a particular percolation threshold, mineralization dictates fiber stiffening[42].

To examine if the morphological and mineralization structural pathologies influence enthesis functionality, a nanoindenter was used to map the viscoelastic material properties across the interface. This modality facilitated testing physiologically relevant loading mechanisms as the FC zones are believed to be predominantly subjected to compression and shearing in that they serve as a stretching-brake[11]. Therefore it is likely imperative to preserve FC functionality in order to maintain meniscus mechanics. Importantly, the OA entheses were significantly more compliant than healthy. As stated prior, changes in bone remodeling and mineralization dictate mechanics. Additionally, degeneration of hydrophilic GAG content results in a loss of resistance to compression. With the various changes exhibited it follows that there would be a demonstrable change in material properties. These changes were observed primarily in both the CFC and UFC regions. Importantly, these

zones are known to be comprised of primarily type II collagen which is severely and irreversibly degraded in early and late stage OA due to an increase in matrix metalloproteinase-13[18,44]. Additionally, the lower bone mineral density in the MA enthesis correlates with the increased compliance.

Previous viscoelastic characterization of osteoarthritic articular cartilage has shown similar losses in viscoelastic properties[45]. These changes have been linked to altered GAG chains, tissue swelling, and collagen cross-linking, which correlate with increased tissue permeability[46-48]. The time-dependent behavior exhibited by cartilage is believed to be driven by both fluid-flow and matrix polymeric mechanisms[49]. Therefore, it is possible that the meniscal entheses, particularly in the fibrocartilaginous zones, exhibit a similar increase in tissue permeability that may have more pronounced effects on the instantaneous tissue response. However, it is difficult to make a definitive statement on these outcomes based on the assays performed.

One shortcoming of the nano-indentation analysis is the assumption of isotropy for clearly anisotropic tissues. However, unlike traditional uniaxial testing, indentation probe techniques are known to somewhat mute the effects of anisotropy, as the modulus derived is representative of a multi-axial measurement. Literature investigating the osteochondral interface uses similar isotropic material assumptions with the caveat that anisotropy may influence the results, however it is not known to what extent at this time[50]. For our study the focus was to leverage the use of this micro-scale technique to determine if any differences were present at discrete locations across the interface. Therefore, this data should be understood solely in the context of comparing the healthy and OA tissue.

Another shortcoming of the indentation testing resides in preparation of the test specimens. It is likely some structural modification results from the processes of embedding, cutting, and sanding. Therefore our results may not be truly representative of the intact native tissue. Additionally, some protocols call for full specimen penetration with plastic resin to stabilize the tissue, however others do not[51]. We opted to not impregnate the tissue and only have an outer shell to ease sample mounting in the test frame. This was performed for fear of masking any differences that would present in the softer tissues when embedding with a stiff resin. Again, this data should be considered only in the comparative context in which it is presented.

An important consideration of this study is the use of end-stage OA tissue. While end-stage OA tissue most likely provided the most contrast with healthy tissue, it cannot be known when the initial breakdown of the enthesis occurred. However, in this initial examination of the meniscal entheses it is apparent that there are deleterious modifications to their structure and function, which may be detrimental to the function of the meniscus. In particular, the MA enthesis exhibited signs of degeneration based on several metrics. This is an intriguing pattern since current literature places emphasis on the medial posterior enthesis due to the clinical incidence of failure[9]. The work presented here however, indicates that structural changes may contribute to altered enthesis functionality. Continued examination of the meniscal entheses and their role in OA pathogenesis may provide new opportunities for arresting OA propagation.

Acknowledgments

This work was supported by grants from the National Institutes of Health (R15 AR051906, 7F31AG039975).

Role of the funding source

The National Institutes of Health had no role in the study design, collection, analysis, or writing of the manuscript.

References

1. Messner K, Gao J. The menisci of the knee joint. anatomical and functional characteristics, and a rationale for clinical treatment. J Anat. 1998; 193(Pt 2):161–78. [PubMed: 9827632]
2. Benjamin M, Evans EJ, Rao RD, Findlay JA, Pemberton DJ. Quantitative differences in the histology of the attachment zones of the meniscal horns in the knee joint of man. J Anat. 1991; 177:127–34. [PubMed: 1769887]
3. Makris EA, Hadidi P, Athanasiou KA. The knee meniscus: structureefunction, pathophysiology, current repair techniques, and prospects for regeneration. Biomaterials. 2011; 32(30):7411–31. [PubMed: 21764438]
4. Setton LA, Guilak F, Hsu EW, Vail TP. Biomechanical factors in tissue engineered meniscal repair. Clin Orthop Relat Res. 1999; 367(Suppl l):S254–72. [PubMed: 10546651]
5. Villegas DF, Haut Donahue TL. Collagen morphology in human meniscal attachments: a SEM study. Connect Tissue Res. 2010; 51(5):327–36. [PubMed: 20388017]
6. Villegas DF, Hansen TA, Liu DF, Haut Donahue TL. A quantitative study of the microstructure and biochemistry of the medial meniscal horn attachments. Ann Biomed Eng. 2008; 36(1):123–31. [PubMed: 17999192]
7. Shaw HM, Benjamin M. Structure–function relationships of entheses in relation to mechanical load and exercise. Scand J Med Sci Sports. 2007; 17(4):303–15. [PubMed: 17490450]
8. Haut Donahue TL, Hull ML, Rashid MM, Jacobs CR. How the stiffness of meniscal attachments and meniscal material properties affect tibio-femoral contact pressure computed using a validated finite element model of the human knee joint. J Biomech. 2003; 36(1):19–34. [PubMed: 12485635]
9. Jones AO, Houang MTW, Low RS, Wood DG. Medial meniscus posterior root attachment injury and degeneration: MRI findings. Australas Radiol. 2006; 50(4):306–13. [PubMed: 16884414]
10. Yao J, Funkenbusch PD, Snibbe J, Maloney M, Lerner AL. Sensitivities of medial meniscal motion and deformation to material properties of articular cartilage, meniscus and meniscal attachments using design of experiments methods. J Biomech Eng. 2006; 128(3):399–408. [PubMed: 16706589]
11. Benjamin M, Toumi H, Ralphs JR, Bydder G, Best TM, Milz S. Where tendons and ligaments meet bone: attachment sites (‘entheses’) in relation to exercise and/or mechanical load. J Anat. 2006; 208(4):471–90. [PubMed: 16637873]
12. Rufai A, Ralphs JR, Benjamin M. Structure and histopathology of the insertional region of the human Achilles tendon. J Orthop Res: Off Publ Orthop Res Soc. 1995; 13(4):585–93.
13. Berthiaume MJ, Raynauld JP, Martel-Pelletier J, Lanobte F, Beaudoin G, Bloch DA, et al. Meniscal tear and extrusion are strongly associated with progression of symptomatic knee osteoarthritis as assessed by quantitative magnetic resonance imaging. Ann Rheum Dis. 2005; 64(4):556–63. [PubMed: 15374855]
14. Costa C, Morrison W. Medial meniscus extrusion on knee MRI: is extent associated with severity of degeneration or type of tear? AJR Am J Roentgenol. 2004; 183(1):17–23. [PubMed: 15208101]
15. Stehling C, Souza RB, Le Graverand MPH, Wyman BT, Li X, Majumdar S, et al. Loading of the knee during 3.0T MRI is associated with significantly increased medial meniscus extrusion in mild and moderate osteoarthritis. Eur J Radiol. 2011:1839–45.
16. Adams JG, McAlindon T, Dimasi M, Carey J, Eustace S. Contribution of meniscal extrusion and cartilage loss to joint space narrowing in osteoarthritis. Clin Radiol. 1999; 54(8):502–6. [PubMed: 10484216]
17. Petersen W, Tillmann B. Collagenous fibril texture of the human knee joint menisci. Anat Embryol. 1998; 197(4):317–24. [PubMed: 9565324]
18. Gao J, Oqvist G, Messner K. The attachments of the rabbit medial meniscus. A morphological investigation using image analysis and immunohistochemistry. J Anat. 1994; 185(Pt 3):663–7. [PubMed: 7649801]
19. Abraham AC, Moyer JT, Villegas DF, Odegard GM, Haut Donahue TL. Hyperelastic properties of human meniscal attachments. J Biomech. 2011; 44(3):413–8. [PubMed: 20980006]
20. Hauch KN, Villegas DF, Haut Donahue TL. Geometry, time-dependent and failure properties of human meniscal attachments. J Biomech. 2010; 43(3):463–8. [PubMed: 19896669]

21. Yao J, Lancianese SL, Hovinga KR, Lee J, Lerner AL. Magnetic resonance image analysis of meniscal translation and tibio-menisco-femoral contact in deep knee flexion. J Orthop Res: Off Publ Orthop Res Soc. 2008; 26(5):673–84.
22. Goldring SR. Role of bone in osteoarthritis pathogenesis. Osteoarthritis. 2009; 93(1):25–35.
23. Goldring MB, Goldring SR. Articular cartilage and subchondral bone in the pathogenesis of osteoarthritis. Ann N Y Acad Sci. 2010; 1192:230–7. [PubMed: 20392241]
24. Sun Y, Mauerhan DR, Honeycutt PR, Jeffrey SK, Norton HJ, Zinchenko N, et al. Calcium deposition in osteoarthritic meniscus and meniscal cell culture. Arthritis Res Ther. 2010; 12(2):R56. [PubMed: 20353559]
25. Oyen ML. Spherical indentation creep following ramp loading. J Mater Res. 2005; 20(08):2094–100.
26. Oyen ML. Nanoindentation of biological and biomimetic materials. Exp Techniques. 2013; 37(1): 73–87.
27. Rho JY, Tsui TY, Pharr GM. Elastic properties of microstructural components of human bone tissue as measured by nanoindentation. J Biomed. 1999; 45(1):48–54.
28. Hauch KN, Oyen ML, Odegard GM, Haut Donahue TL. Nanoindentation of the insertional zones of human meniscal attachments into underlying bone. J Mech Behav Biomed Mater. 2009; 2(4): 339–47. [PubMed: 19627840]
29. Hu K, Radhakrishnan P, Patel RV, Mao JJ. Regional structural and viscoelastic properties of fibrocartilage upon dynamic nanoindentation of the articular condyle. J Struct Biol. 2001; 136(1): 46–52. [PubMed: 11858706]
30. Paietta RC, Campbell SE, Ferguson VL. Influences of spherical tip radius, contact depth, and contact area on nanoindentation properties of bone. J Biomech. 2011; 44(2):285–90. [PubMed: 21092970]
31. Abraham AC, Haut Donahue TL. From meniscus to bone: a quantitative evaluation of structure and function of the human meniscal attachments. Acta Biomater. 2013; 9(5):6322–9. [PubMed: 23385217]
32. Kahn KM, Bonar F, Desmond PM, Cook JL, Visentini PH, Fehrmann MW, et al. Patellar tendinosis (jumper's knee): findings at histopathologic examination, US, and MR imaging. Victorian Institute of Sport Tendon Study Group. Radiology. 1996; 200(3):821–7. [PubMed: 8756939]
33. Meknas K, Johansen O, Steigen SE, Olsen R, Jørgensen L, Kartus J. Could tendinosis be involved in osteoarthritis? Scand J Med Sci Sports. 2012; 22(5):627–34. [PubMed: 21410541]
34. Liu YZ, Jackson AP, Cosgrove SD. Contribution of calcium-containing crystals to cartilage degradation and synovial inflammation in osteoarthritis. OA&C. 2009; 17(10):1333–40.
35. Kumar P, Oka M, Nakamura T, Yamamuro T, Delecrin J. Mechanical strength of osteochondral junction. Nihon Seikeigeka Gakkai Zasshi. 1991; 65(11):1070–7. [PubMed: 1761907]
36. Redler I, Mow VC, Zimny ML, Mansell J. The ultrastructure and biomechanical significance of the tidemark of articular cartilage. Clin Orthop Relat Res. 1975; 112:357–62. [PubMed: 1192647]
37. Smith LR, Fowler-Gerace LH, Gerace-Fowler L, Lieber RL. Muscle extracellular matrix applies a transverse stress on fibers with axial strain. J Biomech. 2011; 44(8):1618–20. [PubMed: 21450292]
38. Burr DB. Anatomy and physiology of the mineralized tissues: role in the pathogenesis of osteoarthrosis. OA&C. 2004; 12(Suppl A):S20–30.
39. Goldring SR. Alterations in periarticular bone and cross talk between subchondral bone and articular cartilage in osteoarthritis. Ther Adv Musculoskelet Dis. 2012; 4(4):249–58. [PubMed: 22859924]
40. Pastoureau P, Leduc S, Chomel A, De Ceuninck F. Quantitative assessment of articular cartilage and subchondral bone histology in the meniscectomized guinea pig model of osteoarthritis. OA&C. 2003; 11(6):412–23.
41. Grynpas MD, Alpert B, Katz I, Lieberman I, Pritzker KP. Subchondral bone in osteoarthritis. Calcif Tissue Int. 1991; 49(1):20–6. [PubMed: 1893292]

42. Genin GM, Kent A, Birman V, Wopenka B, Pasteris JD, Marquez PJ, et al. Functional grading of mineral and collagen in the attachment of tendon to bone. Biophys J. 2009; 97(4):976–85. [PubMed: 19686644]
43. Wopenka B, Kent A, Pasteris J. The tendon-to-bone transition of the rotator cuff: a preliminary Raman spectroscopic study documenting the gradual mineralization across the insertion in rat tissue. Appl Spectrosc. 2008; 62(12):1285–94. [PubMed: 19094386]
44. Goldring MB, Otero M, Darren AP, Dragomir C, Favero M, Hachem KE, et al. Roles of inflammatory and anabolic cytokines in cartilage metabolism: signals and multiple effectors converge upon MMP-13 regulation in osteoarthritis. Eur Cell Mater. 2011; 21:202–20. [PubMed: 21351054]
45. Desrochers J, Amrein MW, Matyas JR. Viscoelasticity of the articular cartilage surface in early osteoarthritis. OA&C. 2012; 20(5):413–21.
46. Ewers BJ, Weaver BT, Sevensma ET, Haut RC. Chronic changes in rabbit retro-patellar cartilage and subchondral bone after blunt impact loading of the patellofemoral joint. J Orthop Res: Off Publ Orthop Res Soc. 2002; 20(3):545–50.
47. Borrelli J, Zaegel MA, Martinez MD, Silva MJ. Diminished cartilage creep properties and increased trabecular bone density following a single, sub-fracture impact of the rabbit femoral condyle. J Orthop Res: Off Publ Orthop Res Soc. 2010; 28(10):1307–14.
48. Bank RA, Soudry M, Maroudas A, Mizrahi J, TeKoppele JM. The increased swelling and instantaneous deformation of osteoarthritic cartilage is highly correlated with collagen degradation. Arthritis Rheum. 2000; 43(10):2202–10. [PubMed: 11037879]
49. Guilak, F.; Butler, D.; Goldstein, SA.; Mooney, D. Functional Tissue Engineering. New York: Srpinger-Verlag; 2003.
50. Thomopoulos, S.; Birman, V.; Genin, G. Structural Interfaces and Attachments in Biology. New York: Springer; 2013.
51. Oyen, ML. Handbook of Nanoindentation: With Biological Applications. Pan Stanford Publishing; 2011.

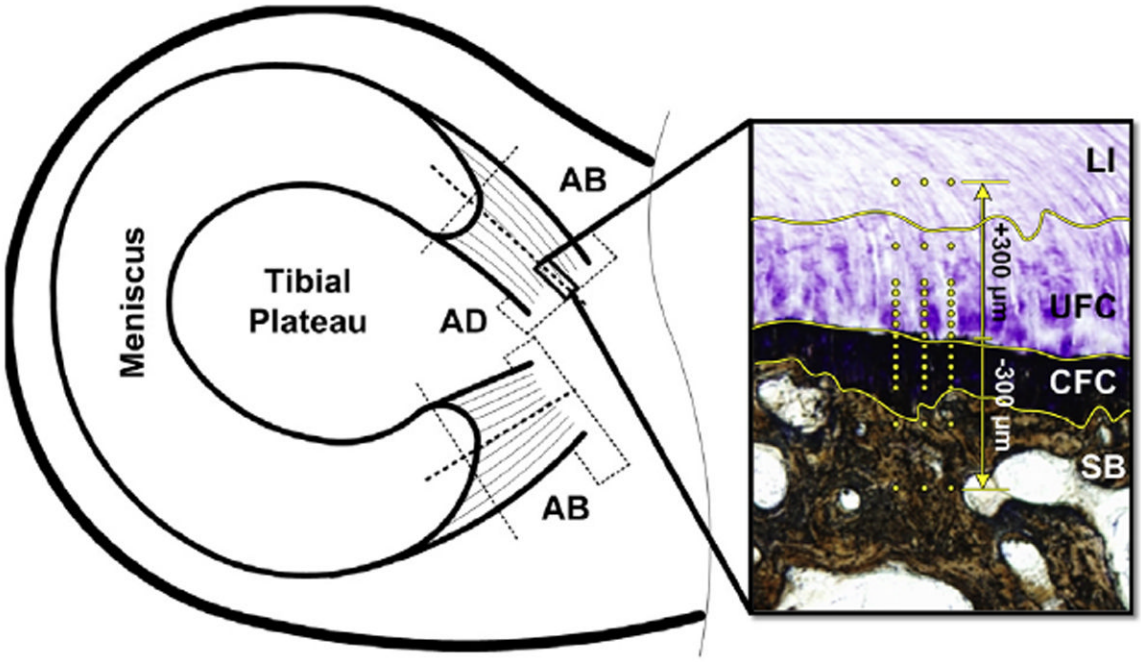

Fig. 1.

Schematic of sample location. AD sections used for histomorphometry. AB sections used for indentation and μCT. Inset – Meniscal enthesis stained with TB/VK to highlight the four unique regions: LI, UFC, CFC, and SB. Yellow lines highlight the demarcations between zones. Yellow dots represent location of indentation test points.

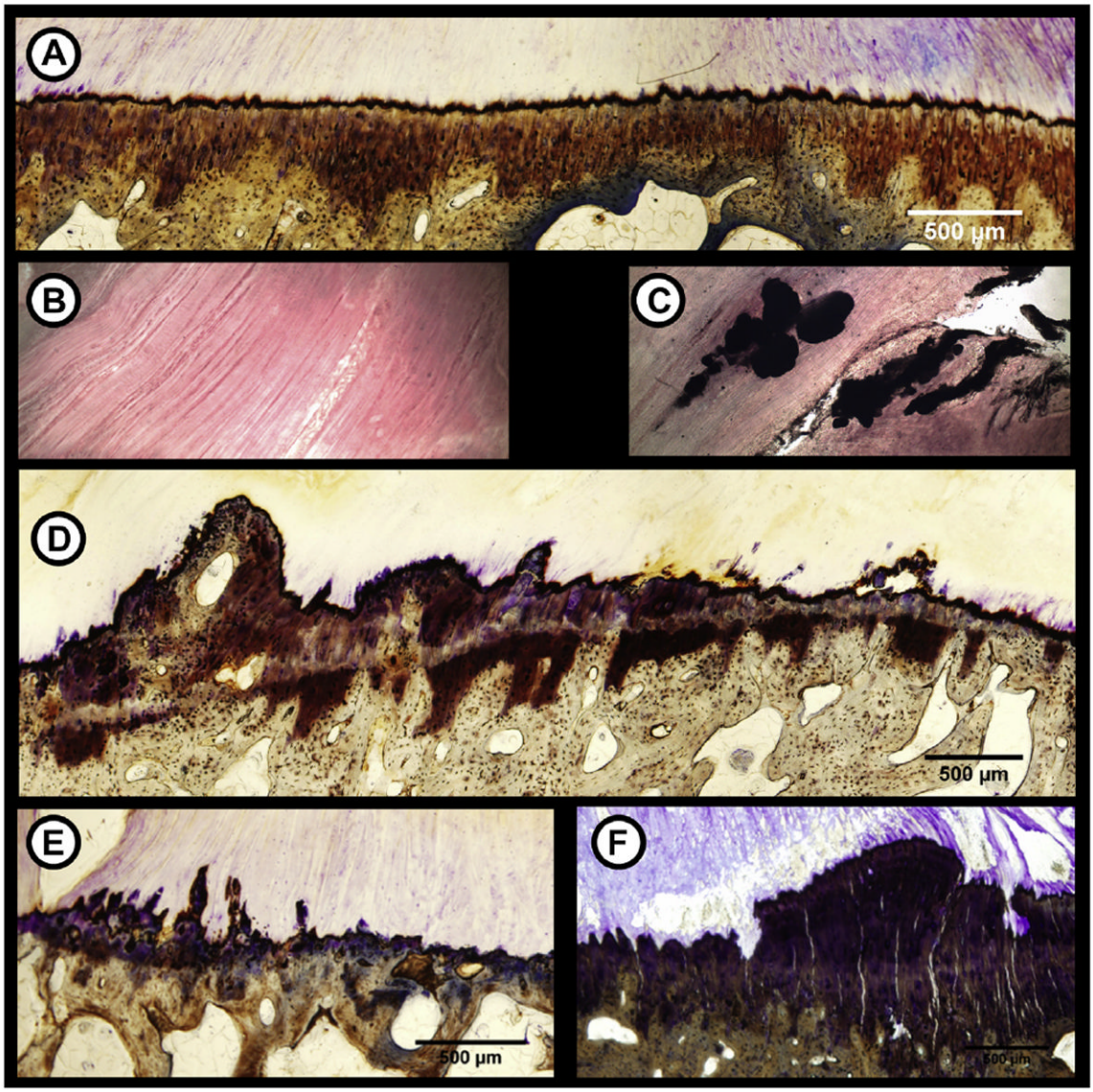

Fig. 2.

Pathophysiology in meniscal entheses due to OA. Healthy entheses have a smooth, intact TM (A) and are free from calcium deposits within the LI portion (B). Osteoarthritic meniscal entheses exhibited degenerative signs similar to other entheses such as calcium deposits within the LI zone (C), double TM formation (D), osteophyte formation (E), and microcracks/fissuring (F).

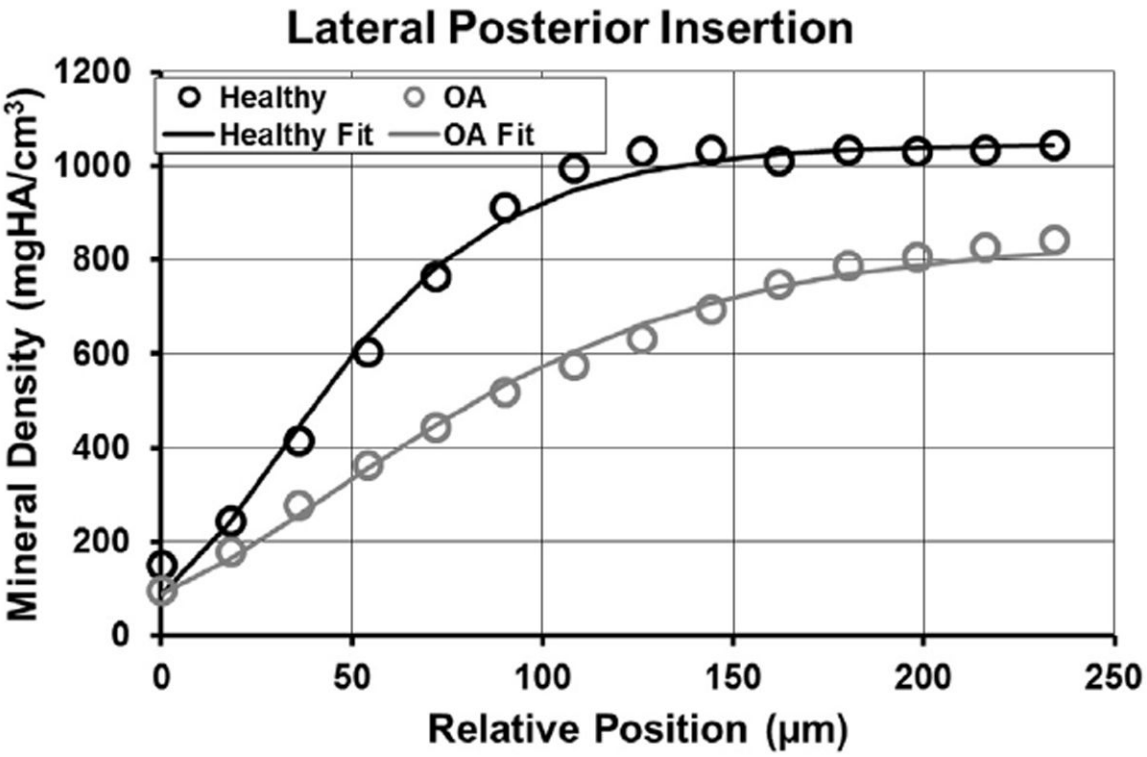

Fig. 3.
Results of fitting the sigmoidal Gompertz function to the mineral density as a function of relative position across the enthesis.

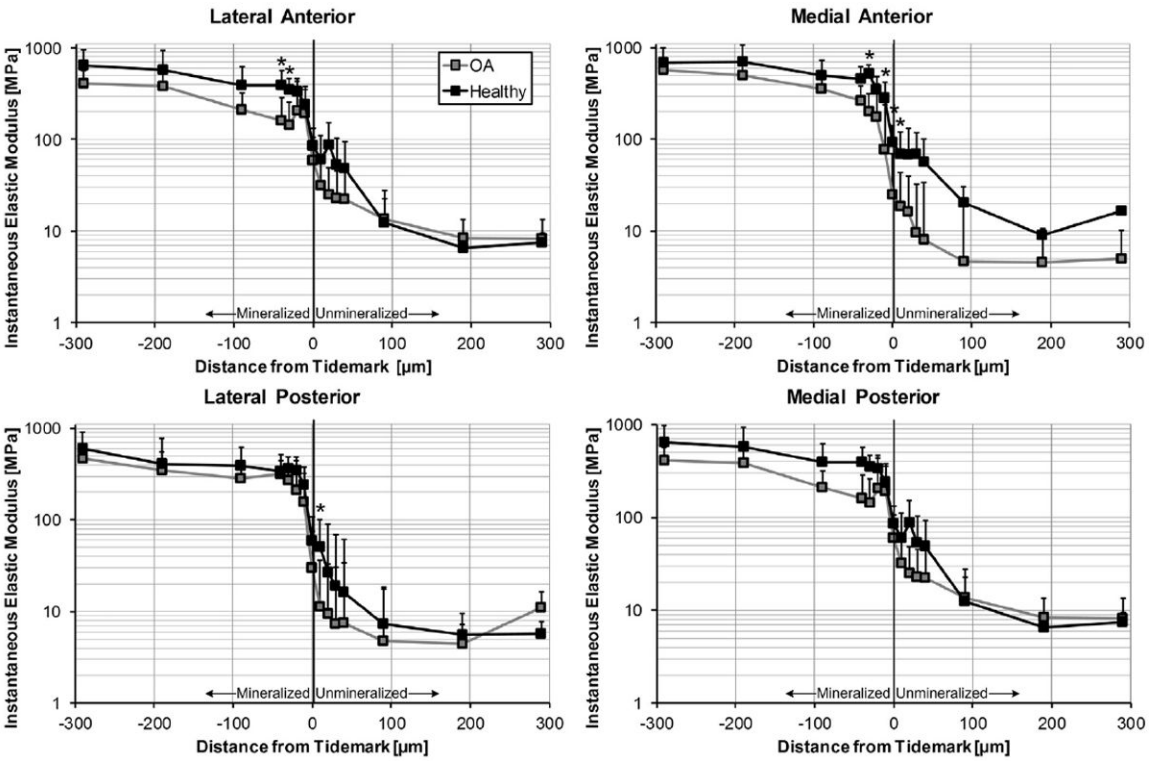

Fig. 4.

Instantaneous elastic modulus as function of relative distance from the TM. Several locations within the fibrocartilaginous zones were significantly more compliant in the arthritic LA, MA, and medial posterior entheses. * – represents significant difference ($P < 0.05$) between healthy and OA tissue for a specific location. Moduli presented as means with 95% confidence interval ($N = 7$ OA knees, $N = 8$ healthy knees, $n = 15$ locations per enthesis).

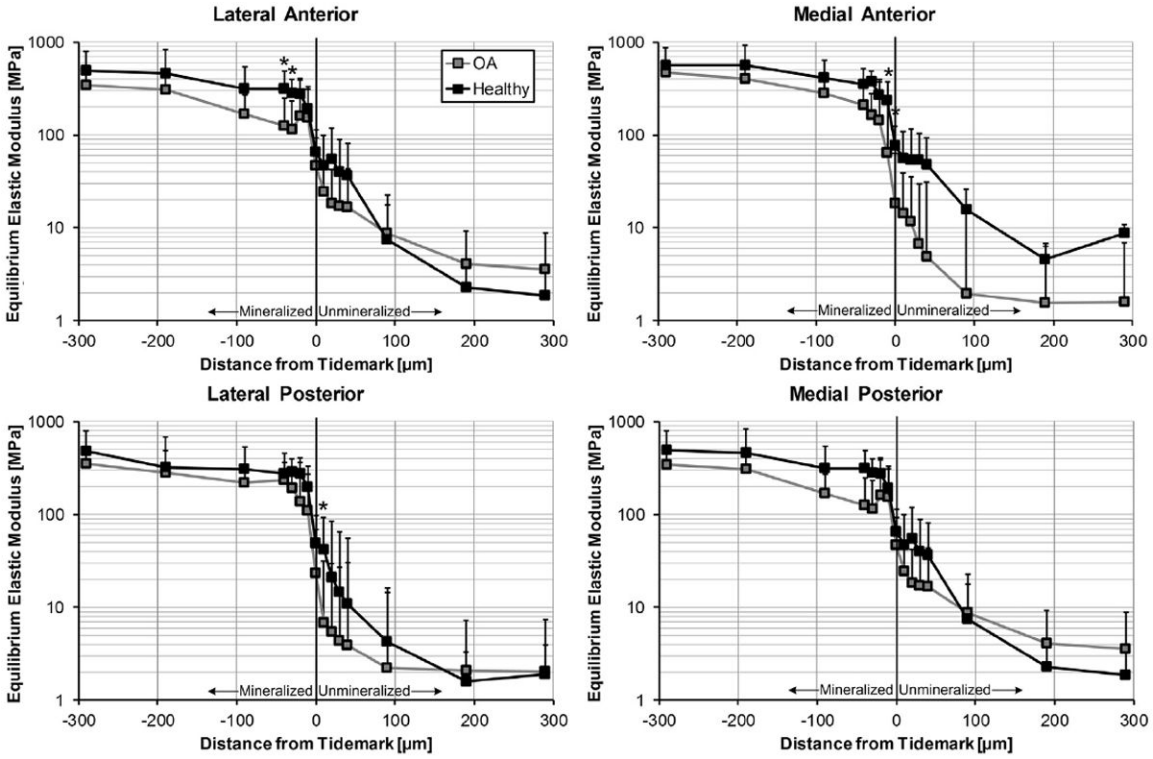

Fig. 5.

Equilibrium elastic modulus as function of relative distance from the TM. Several locations within the fibrocartilaginous zones were significantly more compliant in the arthritic LA, MA, and medial posterior entheses. * – represents significant difference ($P < 0.05$) between healthy and OA tissue for a specific location. Moduli presented as means with 95% confidence interval ($N = 7$ OA knees, $N = 8$ healthy knees, $n = 15$ locations per enthesis).

Table I

Histomorphometry results.

		Calcium deposition	Tidemark integrity		Glycosaminoglycan thickness	
			Variance of first derivate (μm^2)	Mean peak amplitude (μm)	UFC (μm)	CFC (μm)
LA	Healthy	1.03 (0.45, 1.60)*	5.62 (0.16, 11.08)	1.02 (.74, 1.30)	239.68 (187.24, 292.11)	209.21 (164.05, 254.37)*
	OA	2.94 (2.08, 3.80)	14.74 (−2.54, 32.01)	1.63 (0.89, 2.37)	577.26 (211.56, 942.96)	371.91 (142.06, 601.75)
LP	Healthy	0.97 (0.38, 1.57)	8.95 (3.09, 14.80)	1.33 (0.95, 1.72)	745.72 (240.95, 1250.49)	182.89 (153.57, 212.21)
	OA	2.50 (1.11, 3.89)	20.74 (−4.86, 46.34)	1.85 (0.64, 3.05)	809.65 (329.27, 1290.04)	264.04 (184.89, 343.20)
MA	Healthy	1.06 (0.38, 1.73)*	2.59 (0.94, 4.23)*	0.88 (0.69, 1.08)*	265.83 (−15.70, 547.36)	120.95 (65.69, 176.69)*
	OA	2.63 (1.70, 3.55)	17.15 (−1.02, 35.31)	1.85 (0.79, 2.91)	1054.15 (298.72, 1809.57)	226.41 (156.78, 296.03)
MP	Healthy	2.06 (1.27, 2.84)	4.36 (1.77, 6.94)	1.20 (0.95, 1.45)	450.25 (32.88, 867.61)	257.76 (196.19, 319.33)*
	OA	1.63 (0.16, 3.09)	75.09 (−49.00, 199.17)	3.19 (0.17, 6.21)	658.87 (338.40, 979.33)	591.12 (253.48, 928.76)

There was a significant amount of calcium deposition in both anterior entheses. The TM was significantly less organized in the arthritic MA enthesis. GAG thickness was significantly greater in arthritic LA, MA, and MP entheses.

* – represents significant difference ($P < 0.05$) between healthy and OA tissue for a specific enthesis. Mean (95% CI lower limit, upper limit) ($N = 8$ healthy knees, $N = 7$ OA knees)

Table II

μCT results.

		Thickness (μm)	Bone mineral density (mgHA/cm^3)
LA	Healthy	442.72 (396.78, 488.66)*	1006.23 (975.63, 1036.83)*
	OA	780.18 (604.59, 955.76)	898.00 (827.92, 968.07)
LP	Healthy	410.39 (350.03, 470.75)*	1035.14 (970.22, 1100.04)
	OA	745.47 (598.22, 892.71)	988.77 (895.54, 1082.00)
MA	Healthy	346.50 (299.33, 393.67)*	1011.18 (957.10, 1065.26)*
	OA	608.09 (471.17, 745.01)	924.58 (±875.13, 974.02)
MP	Healthy	405.88 (333.49, 478.26)*	1041.98 (1004.52, 1079.44)*
	OA	826.61 (682.72, 970.50)	933.67 (846.48, 1020.86)

The cortical thickness was significantly greater in arthritic LA, LP, MA, and MP entheses. Bone mineral density decreased in arthritic LA, MA, and MP entheses.

* – represents significant difference ($P < 0.05$) between healthy and OA tissue for a specific enthesis. Mean (95% CI lower limit, upper limit). (N = 8 healthy knees, N = 7 OA knees)

Table III

Fitting coefficients for sigmoidal mineral density function.

		A	B	C
LA	Healthy	993.16 (915.16, 1071.15)	−3.37 (−4.55, −2.19)	−0.027 (−0.030, −0.023)
	OA	965.08 (909.10, 1021.21)	−3.78 (−4.77, −2.78)	−0.022 (−0.026, −0.018)
LP	Healthy	1000.20 (919.19, 1081.21)	−5.20 (−8.40, −1.99)	−0.026 (−0.030, −0.022)
	OA	1060.26 (945.19, 1175.34)	−5.17 (−8.05, −2.30)	−0.022 (−0.025, −0.020)
MA	Healthy	911.79 (833.74, 989.85)	−3.26 (−4.55, −1.97)	−0.025 (−0.029, −0.020)
	OA	923.83 (845.53, 1002.12)	−2.97 (−3.52, −2.42)	−0.021 (−0.025, −0.020)
MP	Healthy	966.20 (877.63, 1054.77)	−3.89 (−4.99, −2.79)	−0.026 (−0.033, −0.018)
	OA	1005.38 (901.83, 1108.93)	−5.64 (−9.10, −2.17)	−0.023 (−0.024, −0.022)

A – represents the peak mineral density. B – represents a horizontal shift in the function, indicative of an initially gradual increase in mineral content. C – represents mineral density growth rate. (N = 8 healthy knees, N = 7 OA knees)